Journal of Physics: Condensed Matter

PAPER • **OPEN ACCESS**

Intrinsic exchange bias from interfacial reconstruction in an epitaxial $Ni_xCo_yFe_{3-x-y}O_4$(111)/α-Al_2O_3(0001) thin film family

To cite this article: Detian Yang *et al* 2024 *J. Phys.: Condens. Matter* **36** 505802

OPEN ACCESS
IOP Publishing
Journal of Physics: Condensed Matter
J. Phys.: Condens. Matter **36** (2024) 505802 (7pp)
https://doi.org/10.1088/1361-648X/ad789d

Intrinsic exchange bias from interfacial reconstruction in an epitaxial $Ni_xCo_yFe_{3-x-y}O_4(111)/\alpha\text{-}Al_2O_3(0001)$ thin film family

Detian Yang[1,2], **Yaohua Liu**[3] and **Xiaoshan Xu**[2,4,*]

[1] Shanghai Key Laboratory of High Temperature Superconductors, Department of Physics, Shanghai University, Shanghai 200444, People's Republic of China
[2] Department of Physics and Astronomy, University of Nebraska, Lincoln, NE 68588, United States of America
[3] Second Target Station, Oak Ridge National Laboratory, Oak Ridge, TN 37830, United States of America
[4] Nebraska Center for Materials and Nanoscience, University of Nebraska, Lincoln, NE 68588, United States of America

E-mail: xiaoshan.xu@unl.edu

Received 26 July 2024, revised 22 August 2024
Accepted for publication 9 September 2024
Published 18 September 2024

Abstract

Intrinsic exchange bias is known as the unidirectional exchange anisotropy that emerges in a nominally single-component ferro-(ferri-)magnetic system. In this work, with magnetic and structural characterizations, we demonstrate that intrinsic exchange bias is a general phenomenon in (Ni, Co, Fe)-based spinel oxide films deposited on α-Al_2O_3(0001) substrates, due to the emergence of a rock-salt interfacial layer consisting of antiferromagnetic CoO from interfacial reconstruction. We show that in $Ni_xCo_yFe_{3-x-y}O_4(111)/\alpha\text{-}Al_2O_3(0001)$ films, intrinsic exchange bias and interfacial reconstruction have consistent dependences on Co concentration y, while the Ni and Fe concentration appears to be less important. This work establishes a family of intrinsic exchange bias materials with great tunability by stoichiometry and highlights the strategy of interface engineering in controlling material functionalities.

Supplementary material for this article is available online

Keywords: exchange bias, interfacial reconstruction, spinel oxides, pulsed laser deposition

1. Introduction

At an interface between two oxides of distinctive structural, charge, spin or orbital orders, dramatic reconstruction [1] can be accommodated and induce novel structural, electronic, and magnetic states. Examples include interfacial MnO double layers with charge polarization in $YMnO_3/Al_2O_3$ [2], quasi-2D electron gas between insulating $LaAlO_3$ and $SrTiO_3$ [3], interfacial superconductivity between insulating La_2CuO_4 and metallic $(La, Sr)_2CuO_4$ [4], and ferromagnetic metal state with colossal magnetoresistance in the superlattice of antiferromagnetic insulators $LaMnO_3$ and $SrMnO_3$ [5].

Exchange bias [6, 7] is a unidirectional anisotropy generated by interfacial exchange interaction between a ferromagnet and an antiferromagnet and works as the essential principle of stabilizing soft ferromagnetic components in magnetic read heads and pinning harder reference

* Author to whom any correspondence should be addressed.

layers in spin valve devices. Intrinsic exchange bias [8] is the phenomenon that exchange bias arises in a nominally single-component ferro/ferri-magnetic material grown on a non-magnetic substrate. Without intentional fabrication of antiferromagnetic components, intrinsic exchange bias phenomena can simplify device designs in magnetic storage and spintronics in view of ever-increasing demands for miniaturization and cost-effect device manufacturing. To date, intrinsic exchange bias has been reported in various heterostructures such as $LaNiO_3/LaMnO_3$ superlattices [9], $La_{2/3}Sr_{1/3}MnO_3/LaSrAlO_4$ [10], $SrRuO_3/LaAlO_3$ [11], Fe/MgO [12] and $La_{0.67}Sr_{0.33}MnO_{3-\delta}/SrTiO_3$ [13]. However, most intrinsic exchange bias studies in thin films remain sporadic and provide poor tunability. And none of these reported materials' exchange biases surpass their coercivities, failing to meet the necessary criterion for application.

Transition metal spinel TM_3O_4 (TM = Fe, Co, Ni) such as Fe_3O_4, $CoFe_2O_4$ and $NiCo_2O_4$ have been intensively studied for applications in chemical/biosensors [14], energy storage [15], electromechanical devices [16] and spintronic devices [17, 18], owning to the broad scope of their flexible magnetic, electronic, optical and chemical properties. Despite the large structural difference between cubic TM_3O_4 and rhombohedral α-Al_2O_3, TM_3O_4 thin films such as Fe_3O_4 [19], $CoFe_2O_4$ [20] and $NiCo_2O_4$ [21] can be epitaxially grown on α-Al_2O_3. We have previously reported that, in $CoFe_2O_4(111)/\alpha$-$Al_2O_3(0001)$ and $NiCo_2O_4(111)/\alpha$-$Al_2O_3(0001)$ thin films, an interfacial layer containing the antiferromagnetic CoO develops from interfacial structural reconstruction, where a colossal intrinsic exchange bias as large as 7 kOe and an exchange bias beyond the coercivity are observed, respectively [8, 22]. Here we demonstrate that such intrinsic exchange bias emerges in spinel thin films $Ni_xCo_yFe_{3-x-y}O_4(111)/\alpha$-$Al_2O_3(0001)$ ($0 \leqslant x + y \leqslant 3$) from interfacial reconstruction as the Co concentration y lies in the range $0.15 \leqslant y \leqslant 2$; and are greatly tunable by Co concentration.

2. Experimental methods

(111)-oriented $NiFe_2O_4$, $Ni_{0.95}Co_{0.15}Fe_{1.95}O_4$, $Ni_{0.75}Co_{0.75}Fe_{1.5}O_4$, $Ni_{0.67}CoFe_{1.33}O_4$, $CoFe_2O_4$, $Ni_{0.5}Co_{1.5}FeO_4$, $NiCo_2O_4$, $Ni_{0.15}Co_{2.55}Fe_{0.3}O_4$ thin films were grown on α-Al_2O_3 (0001) substrates by pulsed laser deposition (PLD) with an oxygen pressure of 5 mTorr at 520 °C, 440 °C, 390 °C, 340 °C, 530 °C, 330 °C, 300 °C and 20 °C, respectively. All targets were fabricated by solid state reaction from Fe_2O_3, NiO and Co_2O_3 powders with a purity of higher than 99.9%. The KrF excimer laser of wavelength 248 nm was employed to ablate the targets with a pulse energy of 120 ± 10 mJ and a repetition rate of 4 Hz. Growth temperatures for all materials have been optimized. The growth processes were in-situ monitored by a reflection high energy electron diffraction (RHEED) system. For every sample, we in-situ recorded the RHEED images along $Ni_xCo_yFe_{3-x-y}O_4[\bar{1}\bar{1}2]/\alpha$-$Al_2O_3[1\bar{1}00]$ every second.

The out-of-plane x-ray diffraction (XRD) and x-ray reflectivity (XRR) were conducted by a Rigaku SmartLab x-ray diffractometer (copper K-α source, x-ray wavelength 1.5406 Å); the film thicknesses were extracted from the XRR data. The in-plane crystal structure was studied by analyzing thickness-resolved RHEED patterns.

The magnetic hysteresis loops were measured from 5 K to 300 K in a superconducting quantum interfere device (SQUID) system after being cooled down from 320 K in ±4 T or ±7 T fields. Exchange bias H_E and coercivity H_C are defined conventionally by $|H_{01}+ H_{02}|/2$ and $|H_{01}$-$H_{02}|/2$, respectively, where H_{01} and H_{02} are the two field values at which magnetization $M(H) = 0$.

3. Universality of intrinsic exchange bias in spinel $Ni_xCo_yFe_{3-x-y}O_4$ films

The ideal spinel structure of TM_3O_4 features a face-centred-cubic oxygen ion sublattice with half of its octahedral sites and one eighth of its tetrahedral sites occupied by smaller TM cations [23]. TM cations arrange in such a way that the lattice constant of TM cation sublattice is the twice as much as that of the oxygen ion sublattice. In this work, eight members of $Ni_xCo_yFe_{3-x-y}O_4$ (111) ($0 < x + y \leqslant 3$) thin films, i.e. $NiFe_2O_4$, $Ni_{0.95}Co_{0.15}Fe_{1.95}O_4$, $Ni_{0.75}Co_{0.75}Fe_{1.5}O_4$, $Ni_{0.67}CoFe_{1.33}O_4$, $CoFe_2O_4$, $Ni_{0.5}Co_{1.5}FeO_4$, $NiCo_2O_4$, $Ni_{0.15}Co_{2.55}Fe_{0.3}O_4$, were epitaxially grown on α-$Al_2O_3(0001)$ substrates by PLD and the growth processes were monitored in situ by RHEED. The cation ratios were chosen so that samples have varying concentrations of Fe, Co and Ni; especially the Co ratio covers a large range from 0 to 2.55. The films' spinel structure is confirmed by the θ-2θ scan of XRD of $Ni_xCo_yFe_{3-x-y}O_4$($0 \leqslant x + y \leqslant 3$) films in figure 1(a) and the typical RHEED patterns along two perpendicular in-plane directions shown in figure 1(b) (see figure S1 in supplemental materials for RHEED patterns of all eight $Ni_xCo_yFe_{3-x-y}O_4$ films). In *x*-*y* phase diagram figure 2(a), the emergence of the intrinsic exchange bias of $Ni_xCo_yFe_{3-x-y}O_4$ films is demonstrated, where the red balls denote the film members with exchange bias and the blue balls indicate the members of which no exchange bias were observed. Shown in figures 2(b)–(e) are typical in-plane hysteresis loops of 4 materials measured at 20 K after the samples were cooled down in ±70 kOe fields (for hysteresis loops of more materials, see figure S2 in supplemental materials). Clearly, except $NiFe_2O_4$ and $Ni_{0.15}Co_{2.55}Fe_{0.3}O_4$, all other samples in $Ni_xCo_yFe_{3-x-y}O_4$ series show significant exchange bias. $NiCo_2O_4$ stands out as its H_E surpasses H_C as shown in figure 2(e) [22]. It is worth mentioning that, as shown in figure 3 and discussed in section 3 in the supplementary materials, the relatively thin samples (about 10 nm) of some films such as $Ni_{0.75}Co_{0.75}Fe_{1.5}O_4$ and $Ni_{0.67}CoFe_{1.33}O_4$ demonstrate intriguing large nominal exchange bias of around 10 kOe as a result of the significant vertical shifts of hysteresis loops along the magnetization

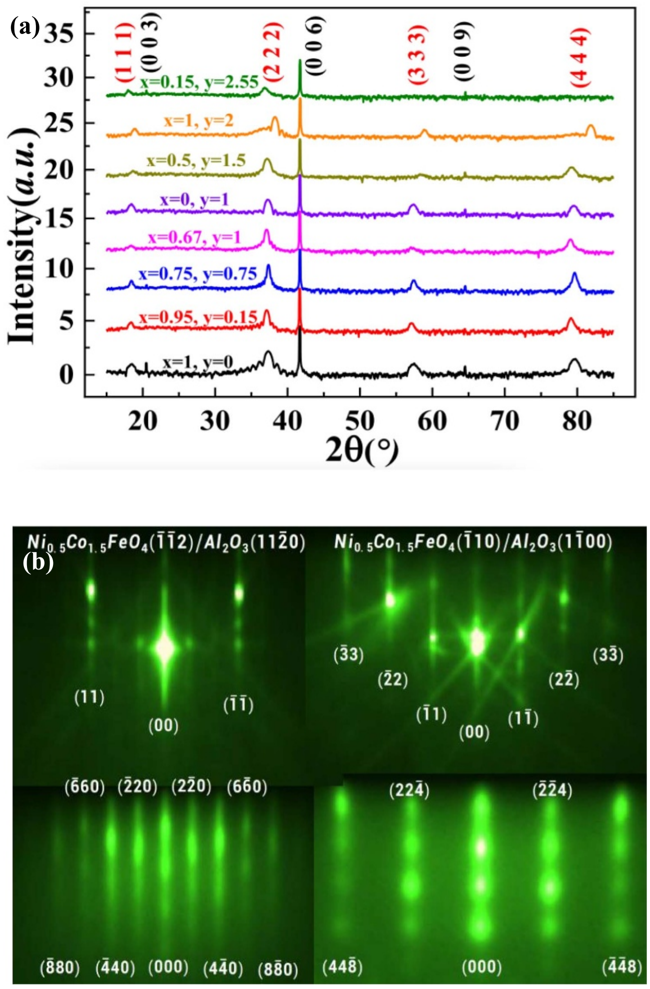

Figure 1. (a) θ-2θ XRD of $Ni_xCo_yFe_{3-x-y}O_4(0 \leqslant x + y \leqslant 3)$ films. The thicknesses of the samples from bottom to top are 11 nm, 18 nm, 32 nm, 21 nm, 13 nm,18 nm, 15 nm and, 18 nm, respectively. (b) RHEED patterns of α-Al_2O_3 and a 18 nm $Ni_{0.5}Co_{1.5}FeO_4$ film along two perpendicular in-plane directions $NiCo_2O_4$ $[\bar{1}10]$ and $[\bar{1}\bar{1}2]$ of the sample in (a).

axis. The inset of figure 2(a) illustrates the proposed realistic structure of $Ni_xCo_yFe_{3-x-y}O_4(111)/\alpha$-$Al_2O_3(0001)$ thin films with an interfacial layer from reconstruction. As already demonstrated in [8, 22], this interfacial layer is proposed to contain antiferromagnetic CoO which pins the magnetization of the ferrimagnetic $Ni_xCo_yFe_{3-x-y}O_4$ layer to produce the intrinsic exchange bias.

4. Interfacial nature and blocking temperature of intrinsic exchange bias

The interfacial nature of intrinsic exchange biases in $Ni_xCo_yFe_{3-x-y}O_4$ thin films is indicated by the thickness-dependence of H_E of $NiCo_2O_4$, $CoFe_2O_4$ and $Ni_{0.75}Co_{0.75}Fe_{1.5}O_4$ in figure 3(a), where t_{FM}, t_I, and t, are the thickness of the ferrimagnetic part of the film, the interfacial layer, and the whole film, respectively. Here, $CoFe_2O_4$ samples were grown in 10 m Torr O_2, while $NiCo_2O_4$ and $Ni_{0.75}Co_{0.75}Fe_{1.5}O_4$ samples were grown in 5 m Torr O_2. Evidently, as the thickness increases, H_E of all three materials decrease steadily here. $H_E(t_{FM})$ of all cases can be fitted into the power law relations with a power of 0.9, 0.4 and 0.5 for $NiCo_2O_4$, $CoFe_2O_4$ and $Ni_{0.75}Co_{0.75}Fe_{1.5}O_4$, respectively. The deviation from the power 1 in the traditional Meiklejohn-Bean model [6] could be due to the smearing interface between the interfacial layer and the ferrimagnetic layer, which will be shown in figure 4.

Temperature-dependent exchange bias and coercivity of a 10 nm $NiCo_2O_4$ film, a 10 nm $CoFe_2O_4$ film and a 12 nm $Ni_{0.75}Co_{0.75}Fe_{1.5}O_4$ film in figure 3(b) demonstrate that both H_E and H_C in general increase with the decreasing of the temperature except the abrupt drops in H_E and H_C for $T < 20$ K in $NiCo_2O_4$ and $CoFe_2O_4$ films coinciding with the sharp jump of their saturation magnetizations for $T < 20$ K in figure 3(c). Presumably, this phenomenon could be a magnetic phase transition from the low-spin state to the high spin state. It might be induced by the strain effect because it was not observed in thick samples. Note that such dramatic changes of H_E, H_C and M_S for $T < 20$ K were not observed in the case of $Ni_{0.75}Co_{0.75}Fe_{1.5}O_4$ (figures 3(b) and (c)), which implies that such a transition is closely related to the stoichiometry of the films. Since thermal energy can disrupt magnetic order and so weaken the interfacial exchange coupling, exchange bias normally can only survive below certain temperature, which is known as the blocking temperature of exchange bias. From figure 3(b), clearly, the blocking temperatures of H_E for all three materials are consistently around 300 K, suggesting a similar or same exchange bias mechanism. Since according to figure 3(c), room-temperature magnetizations of all three kinds of thin films stay still quite large, the Curie temperatures of $NiCo_2O_4$, $CoFe_2O_4$ and $Ni_{0.75}Co_{0.75}Fe_{1.5}O_4$ are expected to go way beyond 300 K. Therefore, the blocking temperatures here mainly reflect the degradation of the interfacial layer's antiferromagnetic order, and so, are supposed to be close to the Néel temperatures of the presumptive antiferromagnetic interfacial layer. Common antiferromagnetic oxides of Fe, Co and Ni include α-Fe_2O_3 ($T_N \sim 950$ K) [24], FeO ($T_N \sim 190$ K) [25], CoO ($T_N \sim 290$ K) [26], Co_3O_4 ($T_N \sim 40$ K) [27] and NiO ($T_N \sim 90$ K) [28]. As only the Néel temperature of CoO matches the vanishing temperature of H_E in the figure 3(b), this supports the structural model in the inset of figure 2(a) with an interfacial layer dominated by CoO.

5. Interfacial reconstruction in $Ni_xCo_yFe_{3-x-y}O_4(111)/\alpha$-$Al_2O_3(0001)$

To reveal the interfacial reconstruction in these $Ni_xCo_yFe_{3-x-y}O_4(111)/\ \alpha$-$Al_2O_3(0001)$ thin films, we recorded thickness-resolved RHEED patterns in situ along the $Ni_xCo_yFe_{3-x-y}O_4$ $[\bar{1}10]$ in-plane direction. For each thickness, the intensity of RHEED image is summed along the streak direction; thickness-resolved RHEED pattern is then obtained by combing the results of different thicknesses, as shown in figure 4(a) for $Ni_{0.5}Co_{1.5}FeO_4$ as an example

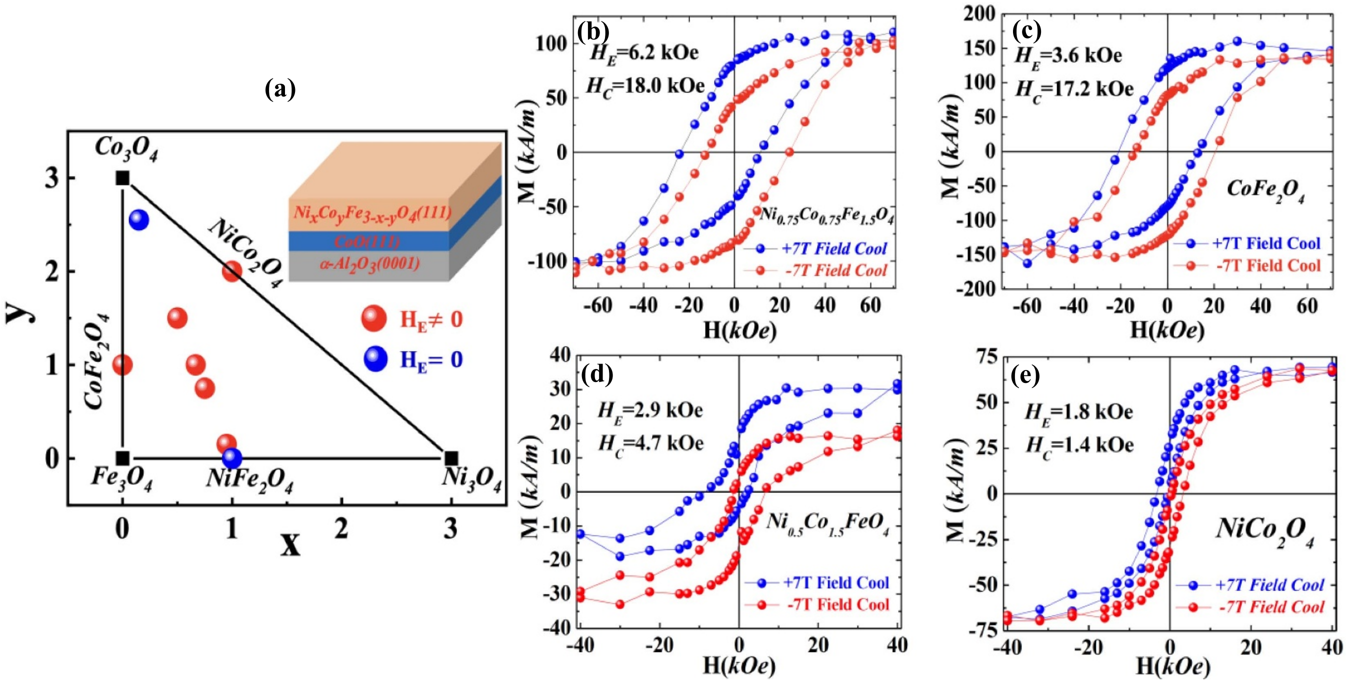

Figure 2. (a) Emergence of Intrinsic exchange bias in spinel $Ni_xCo_yFe_{3-x-y}O_4$ ($0 \leqslant x + y \leqslant 3$) thin films shown in the x-y phase diagram. The films in which nonzero exchange bias ($H_E \neq 0$) was observed are denoted by red solid circles, while those do not exhibit exchange bias ($H_E = 0$) by blue solid circles. Experimentally, any exchange bias value smaller than 0.2 kOe was taken as a result of experimental errors. The inset represents the proposed structure of $Ni_xCo_yFe_{3-x-y}O_4$ thin films with an interfacial layer shown with the blue color. (b)–(e) Featured magnetic in-plane hysteresis loops of $Ni_xCo_yFe_{3-x-y}O_4$ films (grown in 5 mTorr oxygen gas) measured at 20 K after cooling in ± 7 T fields: (b) 16 nm $Ni_{0.75}Co_{0.75}Fe_{1.5}O_4$; (c) 9 nm $CoFe_2O_4$; (d) 11 nm $Ni_{0.5}Co_{1.5}FeO_4$; (e) 10 nm $NiCo_2O_4$. H_E and H_C are exchange bias and coercivity, respectively. The data in (e) was also published previously by the authors in [22].

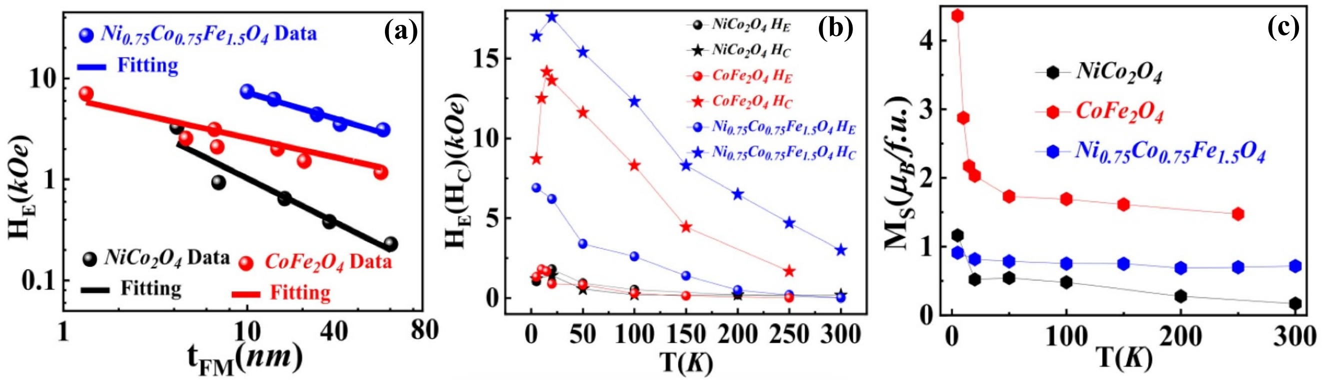

Figure 3. (a) Thickness-dependent exchange bias H_E (circles) and their fittings (lines) of $NiCo_2O_4$ (black), $CoFe_2O_4$ (red) and $Ni_{0.75}Co_{0.75}Fe_{1.5}O_4$ (blue); the data of $NiCo_2O_4$ was measured at 50 K with +40 kOe cooling field, while those of $CoFe_2O_4$ and $Ni_{0.75}Co_{0.75}Fe_{1.5}O_4$ at 20 K with +70 kOe cooling field. $t_{FM} = t - t_I$ is the ferrimagnetic layer thickness with the interfacial layer thickness t_I subtracted from the total thickness t. (b) Temperature behaviors of exchange bias H_E (circles) and coercivity H_C (stars) of a 10 nm $NiCo_2O_4$ (black), 10 nm $CoFe_2O_4$ (red) and a 12 nm $Ni_{0.75}Co_{0.75}Fe_{1.5}O_4$ (blue). (c) Temperature behaviors of saturation moments M_S of a 10 nm $NiCo_2O_4$ (black), a 10 nm $CoFe_2O_4$ (red) and a 12 nm $Ni_{0.75}Co_{0.75}Fe_{1.5}O_4$ (blue). The data about $CoFe_2O_4$ films here were also published previously by the authors in [8].

(see figure S5 for all materials in supplementary materials). As illustrated in figure 4(a), the interfacial-layer stands out without obvious RHEED lines (2 2 −4) and (−2 −2 4) of the spinel structure and the distances between (4 4 −8) and (−4 −4 8) lines in interfacial-layer are smaller than that of spinel $Ni_{0.5}Co_{1.5}FeO_4$, matching the crystal structure and lattice constants of FeO, CoO and/or NiO. To quantify the differences between the interfacial layer and the well-defined $Ni_{0.5}Co_{1.5}FeO_4$, from figure 4(a), we extract the thickness dependence of the in-plane lattice constant relative to the thick-limit value, and the intensity of RHEED lines (2 2 −4). Figure 4(b) corresponds to the $Ni_{0.5}Co_{1.5}FeO_4$ film in the range $0 < t < 6.5$ nm. The profiles of in-plane lattice constant and RHEED line (2 2 −4) intensity in figure 4(b) indicate that

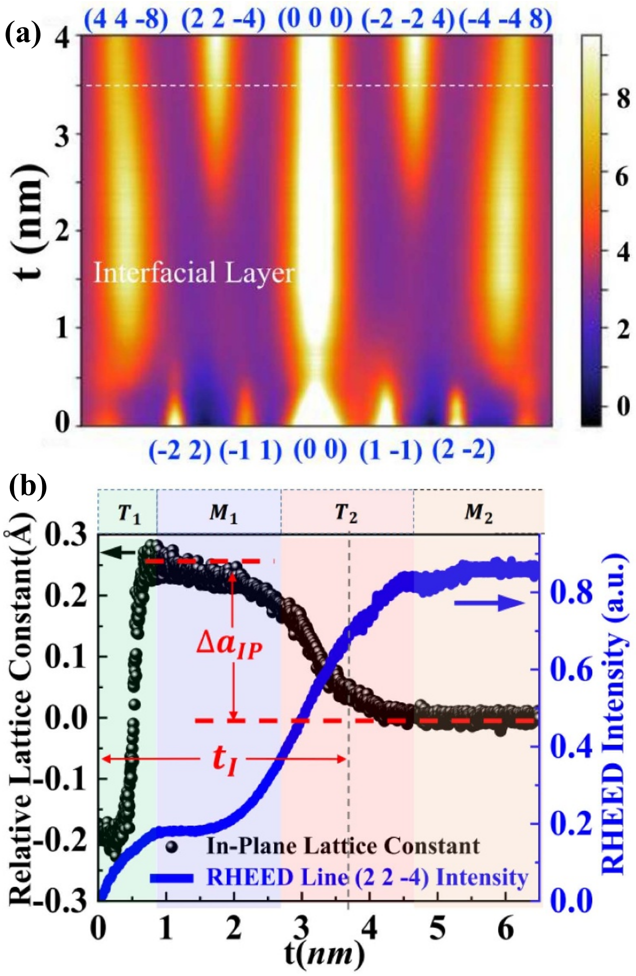

Figure 4. (a) Typical thickness-resolved RHEED patterns of a $Ni_{0.5}Co_{1.5}FeO_4$ sample along the in-plane direction $[\bar{1}10]$; the white dashed lines mark the boundaries of interfacial layers defined later in (b). (b) Thickness-dependent relative in-plane lattice constant (black circles) and (2 2 −4) RHEED line intensity (blue curve) extracted from (a); the interfacial layer contains one main sublayer M_1 (bluish region) with larger lattice constant, transition layer T_1 (greenish region) between substrate and M_1 and transition layer T_2 (reddish region) between M_1 and second main layer $Ni_{0.5}Co_{1.5}FeO_4$ M_2; Δa_{IP} is the in-plane lattice constant difference between the main sublayer M_1 and second main layer $Ni_{0.5}Co_{1.5}FeO_4$ M_2; The in-plane lattice constant of M_2 was chosen as the baseline.

the interfacial layer at least includes three sublayers: one main sublayer M_1 (bluish region) with a larger lattice constant, a transition layer T_1 (greenish region) between the substrate and M_1, and a second transition layer T_2 (reddish region) between M_1 and the second main layer M_2. Both the RHEED pattern and the lattice constant of the M_1 sublayer match the rock-salt structure of FeO, CoO and NiO. Since PLD growth tends to keep the cation ratio from the $Ni_xCo_yFe_{3-x-y}O_4$ target, T_1 and M_1 are plausibly some mixtures of FeO, CoO and NiO according to the chemical formula $Ni_xCo_yFe_{3-x-y}O_4$. In figure 4(b), we defined two quantities to characterize the interfacial reconstruction: the interfacial layer thickness $t_I$is defined as the sum of the thicknesses of T_1, M_1 and half of T_2 with half of T_2 as the error bar, and Δa_{IP} as the in-plane lattice constant difference between M_1 and M_2.

6. The role of Co

With both magnetic and structural characterizations, we have demonstrated that an interfacial layer tends to emerge between the substrate and the ferrimagnetic $Ni_xCo_yFe_{3-x-y}O_4$ films as $0.15 \leqslant y \leqslant 2$ and contains CoO as the essential component to produce the observed exchange bias. In this section, we provide more evidence and analyses in terms of cation concentrations.

Figure 2(a) already suggests that Co plays a key role in the mechanism of exchange bias: by comparing $NiFe_2O_4$ and $Ni_{0.95}Co_{0.15}Fe_{1.95}O_4$, slight doping of Co leads to emergence of exchange bias, while over-doping of Co eliminates the intrinsic exchange bias phenomenon again as seen from the case of $Ni_{0.15}Co_{2.55}Fe_{0.3}O_4$. To quantify the unique role of Co in the mechanism of exchange bias and interfacial reconstruction, we extract from figure 2(a) and thickness-resolved RHEED data the dependence of H_E, t_I and Δa_{IP} on the cation concentrations and plot them in figures 5(a)–(c). Because the magnitudes of exchange bias values are sensitive to the specific ferromagnetic components, they vary dramatically among different $Ni_xCo_yFe_{3-x-y}O_4$ samples as we already seen in figures 2 and S2. In figure 5(a). We therefore focus on whether the cation concentrations correlate with the emergence of exchange bias or not, for which we indicate using P (positive) and N (null) respectively. As defined above, t_I and Δa_{IP} characterize structural interfacial reconstruction. Based on figure 5, the dependence of exchange bias and interfacial reconstruction on Ni concentration x and Fe concentration $3-x-y$ exhibit no obvious trends. In particular, t_I and Δa_{IP} can take two considerably distinctive values in two different materials $NiFe_2O_4$ and $NiCo_2O_4$ of the same Ni concentration $x = 1$. On the other hand, H_E, t_I and Δa_{IP} appear to have a consistent dependence on the Co concentration y: H_E, t_I and Δa_{IP} approach zero at $y = 0$ and $y = 2.55$, while they stay finite in the range $0.15 \leq y \leq 2$. This consistency reveals the key role of Co in the interfacial reconstruction mechanism. Moreover, since $Ni_{0.67}CoFe_{1.33}O_4$ and $CoFe_2O_4$ show similar t_I and Δa_{IP} values (two $y = 1$ points in figures 5(b) and (c)), Ni and Fe concertation seem less critical in the interfacial reconstruction. The matching t_I-y and Δa_{IP}-y relations further suggest that Co concentration dominates the modulation of the lattice constant and the thickness of the interfacial layer by modulating the reconstruction process. In terms of the growth process, our results here and in [22] reveal that, when oxygen vacancy increases (low growth oxygen pressure), Co rather than Fe and Ni tends to be able to initiate the rock-salt interfacial layer over the c-plane of α-Al_2O_3. The apparent counter example for $y = 2.55$, might be a result of the worse crystallization in its growth as indicated by the weak and incomplete XRD (111) peaks of $Ni_{0.15}Co_{2.55}Fe_{0.3}O_4$ in figure 1(a); it is also plausible that the reconstruction mechanism alters significantly once Co concentration surpasses certain value.

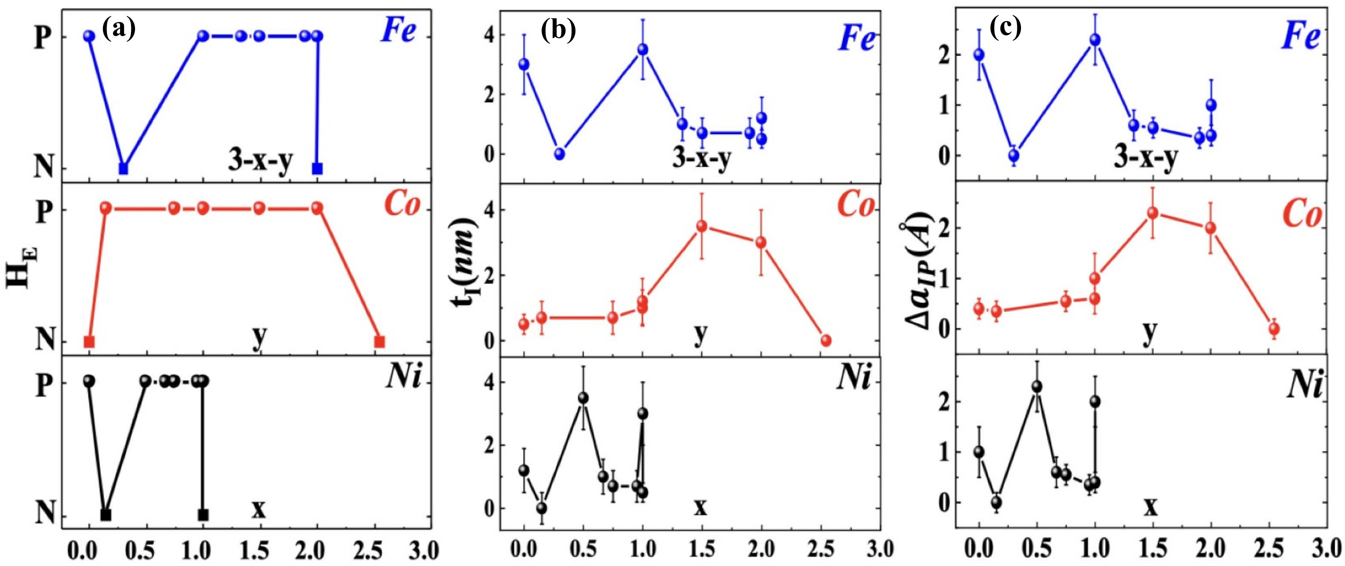

Figure 5. The dependence of exchange bias H_E (a), interfacial layer thickness t_I (b) and the relative in-plane lattice constant of the interfacial layer Δa_{IP} (c) on the concentration of Fe (top panels), Co (middle panels) and Ni (bottom panels). In (a), balls denote that substantial exchange bias larger than 0.2 kOe was observed (*P*) for certain thin films, while squares stand for a null exchange bias value (*N*) for certain thin films. $t_I$and Δa_{IP} were extracted from figure S5.

Although the microscopic mechanism of the interfacial reconstruction in $Ni_xCo_yFe_{3-x-y}O_4$ thin film family requires further experimental and theoretical studies, the analysis in this section clearly supports the aforementioned exchange bias mechanism, i.e. antiferromagnetic CoO in the interfacial layer couples with ferrimagnetic $Ni_xCo_yFe_{3-x-y}O_4$ to generate the exchange bias.

7. Conclusions

In conclusion, we have established a spinel oxide thin film family $Ni_xCo_yFe_{3-x-y}O_4(111)/\alpha\text{-}Al_2O_3(0001)$ to generate and study intrinsic exchange bias. The intrinsic exchange bias was demonstrated to be produced by an antiferromagnetic interfacial layer, in which the effect of CoO dominates. The exchange bias and interfacial reconstruction could be tuned greatly by many parameters including thickness, temperature, growth oxygen pressure and cation concentrations. Thanks to the versatile properties of $Ni_xCo_yFe_{3-x-y}O_4$ ranging from ferrimagnetic semimetal to antiferromagnetic insulator, this thin film family holds promising potential for applications in magnetic storage devices and spintronic devices.

Data availability statement

All data that support the findings of this study are included within the article (and any supplementary files).

Acknowledgment

The authors acknowledge the primary support from the National Science Foundation (NSF) through EPSCoR RII Track-1: Emergent Quantum Materials and Technologies (EQUATE), Award No. OIA-2044049. The research was performed in part in the Nebraska Nanoscale Facility: National Nanotechnology Coordinated Infrastructure and the Nebraska Center for Materials and Nanoscience, which are supported by the NSF under Grant Nos. ECCS-2025298, and the Nebraska Research Initiative.

ORCID iDs

Detian Yang https://orcid.org/0000-0001-8807-3041
Yaohua Liu https://orcid.org/0000-0002-5867-5065
Xiaoshan Xu https://orcid.org/0000-0002-4363-392X

References

[1] Hwang H Y, Iwasa Y, Kawasaki M, Keimer B, Nagaosa N and Tokura Y 2012 Emergent phenomena at oxide interfaces *Nat. Mater.* **11** 103
[2] Cheng S *et al* 2018 Interface reconstruction with emerging charge ordering in hexagonal manganite *Sci. Adv.* **4** eaar4298
[3] Thiel S, Hammerl G, Schmehl A, Schneider C W and Mannhart J 2006 Tunable quasi-two-dimensional electron gases in oxide heterostructures *Science* **313** 1942
[4] Gozar A, Logvenov G, Kourkoutis L F, Bollinger A T, Giannuzzi L A, Muller D A and Bozovic I 2008 High-temperature interface superconductivity between metallic and insulating copper oxides *Nature* **455** 782
[5] Bhattacharya A, May S J, Te Velthuis S G E, Warusawithana M, Zhai X, Jiang B, Zuo J M, Fitzsimmons M R, Bader S D and Eckstein J N 2008 Metal-insulator transition and its relation to magnetic structure in $(LaMnO_3)_{2n}/(SrMnO_3)_n$ superlattices *Phys. Rev. Lett.* **100** 257203
[6] Nogués J, Sort J, Langlais V, Skumryev V, Suriñach S, Muñoz J S and Baró M D 2005 Exchange bias in nanostructures *Phys. Rep.* **422** 65

[7] Zhang W and Krishnan K M 2016 Epitaxial exchange-bias systems: from fundamentals to future spin-orbitronics *Mater. Sci. Eng.* R **105** 1–20

[8] Yang D, Yun Y, Subedi A, Rogers N E, Cornelison D M, Dowben P A and Xu X 2021 Colossal intrinsic exchange bias from interfacial reconstruction in epitaxial $CoFe_2O_4/Al_2O_3$ thin films *Phys. Rev.* B **103** 224405

[9] Gibert M, Zubko P, Scherwitzl R, Íñiguez J and Triscone J M 2012 Exchange bias in $LaNiO_3$-$LaMnO_3$ superlattices *Nat. Mater.* **11** 195

[10] Cui B, Song C, Wang G Y, Mao H J, Zeng F and Pan F 2013 Strain engineering induced interfacial self-assembly and intrinsic exchange bias in a manganite perovskite film *Sci. Rep.* **3** 2542

[11] Sow C, Pramanik A K and Anil Kumar P S 2014 Exchange bias in strained $SrRuO_3$ thin films *J. Appl. Phys.* **116** 194310

[12] Fan Y, Smith K J, Lüpke G, Hanbicki A T, Goswami R, Li C H, Zhao H B and Jonker B T 2013 Exchange bias of the interface spin system at the Fe/MgO interface *Nat. Nanotechnol.* **8** 438

[13] Schumacher D, Steffen A, Voigt J, Schubert J, Brückel T, Ambaye H and Lauter V 2013 Inducing exchange bias in $La_{0.67}Sr_{0.33}MnO_{3-\delta}/SrTiO_3$ thin films by strain and oxygen deficiency *Phys. Rev.* B **88** 144427

[14] Su C 2017 Environmental implications and applications of engineered nanoscale magnetite and its hybrid nanocomposites: a review of recent literature *J. Hazard. Mater.* **322** 48

[15] An Q, Lv F, Liu Q, Han C, Zhao K, Sheng J, Wei Q, Yan M and Mai L 2014 Amorphous vanadium oxide matrixes supporting hierarchical porous Fe_3O_4/graphene nanowires as a high-rate lithium storage anode *Nano Lett.* **14** 6250

[16] Wang X, Liao Y, Zhang D, Wen T and Zhong Z 2018 A review of Fe_3O_4 thin films: synthesis, modification and applications *J. Mater. Sci. Technol.* **34** 1259

[17] Ramos A V, Santos T S, Miao G X, Guittet M J, Moussy J B and Moodera J S 2008 Influence of oxidation on the spin-filtering properties of $CoFe_2O_4$ and the resultant spin polarization *Phys. Rev.* B **78** 180402

[18] Xu X, Mellinger C, Cheng Z G, Chen X and Hong X 2022 Epitaxial $NiCo_2O_4$ film as an emergent spintronic material: magnetism and transport properties *J. Appl. Phys.* **132** 020901

[19] Bataille A M, Ponson L, Gota S, Barbier L, Bonamy D, Gautier-Soyer M, Gatel C and Snoeck E 2006 Characterization of antiphase boundary network in Fe_3O_4 (111) epitaxial thin films: effect on anomalous magnetic behaviour *Phys. Rev.* B **74** 155438

[20] Ramos A V, Moussy J B, Guittet M J, Gautier-Soyer M, Gatel C, Bayle-Guillemaud P, Warot-Fonrose B and Snoeck E 2007 Influence of a metallic or oxide top layer in epitaxial magnetic bilayers containing $CoFe_2O_4$(111) tunnel barriers *Phys. Rev.* B **75** 224421

[21] Zhen C, Zhang X, Wei W, Guo W, Pant A, Xu X, Shen J, Ma L and Hou D 2018 Nanostructural origin of semiconductivity and large magnetoresistance in epitaxial $NiCo_2O_4/Al_2O_3$ thin films *J. Phys. D: Appl. Phys.* **51** 145308

[22] Yang D, Subedi A, Liu C, Ambaye H, Laiter V, Dowben P A, Liu Y and Xu X 2024 Microstructural underpinnings of giant intrinsic exchange bias in epitaxial $NiCo_2O_4$ thin films (arXiv:2302.13227v4[cond-mat.mtrl-sci])

[23] Sickafus K E, Wills J M and Grimes N W 1999 Structure of spinel *J. Am. Ceram. Soc.* **82** 3279

[24] Białek M, Zhang J, Yu H and Ansermet J P 2022 Antiferromagnetic resonance in α-Fe_2O_3 up to its Néel temperature *Appl. Phys. Lett.* **121** 032401

[25] Roth W L 1958 Magnetic Structures of MnO, FeO, CoO, and NiO *Phys. Rev.* **10** 1333

[26] Tang Y J, Zink B L, Hellman F, Berkowitz A E, Tang Y J, Hellman F, Berkowitz A E and Smith D J 2003 Finite size effects on the moment and ordering temperature in antiferromagnetic CoO layers *Phys. Rev.* B **67** 054408

[27] Dutta P, Seehra M S, Thota S and Kumar J 2008 A comparative study of the magnetic properties of bulk and nanocrystalline Co_3O_4 *J. Phys.: Condens. Matter* **20** 015218

[28] Barbier A, Mocuta C, Neubeck W, Mulazzi M, Yakhou F, Chesnel K, Sollier A, Vettier C and De Bergevin F 2004 Surface and bulk spin ordering of antiferromagnetic materials: niO(111) *Phys. Rev. Lett.* **93** 257208